

# Nanoscale

Accepted Manuscript



This is an *Accepted Manuscript*, which has been through the Royal Society of Chemistry peer review process and has been accepted for publication.

*Accepted Manuscripts* are published online shortly after acceptance, before technical editing, formatting and proof reading. Using this free service, authors can make their results available to the community, in citable form, before we publish the edited article. We will replace this *Accepted Manuscript* with the edited and formatted *Advance Article* as soon as it is available.

You can find more information about *Accepted Manuscripts* in the [Information for Authors](#).

Please note that technical editing may introduce minor changes to the text and/or graphics, which may alter content. The journal's standard [Terms & Conditions](#) and the [Ethical guidelines](#) still apply. In no event shall the Royal Society of Chemistry be held responsible for any errors or omissions in this *Accepted Manuscript* or any consequences arising from the use of any information it contains.

Dendrimer-Encapsulated Naphthalocyanine as a Single Agent-Based Theranostic Nanoplatfrom  
for Near-Infrared Fluorescence Imaging and Combinatorial Anticancer Phototherapy

Olena Taratula, Canan Schumann, Tony Duong, Karmin L. Taylor, and Oleh Taratula\*

*Department of Pharmaceutical Sciences, College of Pharmacy, Oregon State University,  
Corvallis, Oregon 97331, United States*

\*Corresponding author. Tel.: +1 541 737 5785 Fax: 541-737-3999

E-mail address: [Oleh.Taratula@oregonstate.edu](mailto:Oleh.Taratula@oregonstate.edu)

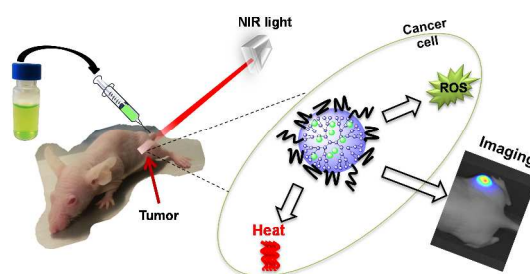
### **Abstract**

Multifunctional theranostic platforms capable of concurrent near-infrared (NIR) fluorescence imaging and phototherapies are strongly desired for cancer diagnostic and treatment. However, integration of separate imaging and therapeutic components into nanocarriers results in complex theranostic systems with limited translational potential. A single agent-based theranostic nanoplatfrom, therefore, was developed for concurrent NIR fluorescence imaging and combinatorial phototherapy with dual photodynamic (PDT) and photothermal (PTT) therapeutic mechanisms. The transformation of substituted silicon naphthalocyanine (SiNc) into biocompatible nanoplatfrom (SiNc-NP) was achieved by SiNc encapsulation into the hydrophobic interior of the generation 5 polypropylenimine dendrimer following surface modification with polyethylene glycol. Encapsulation provides aqueous solubility to SiNc and preserves its NIR fluorescence, PDT and PTT properties. Moreover, impressive photostability of dendrimer-encapsulated SiNc have been detected. Under NIR irradiation (785 nm, 1.3 W/cm<sup>2</sup>), SiNc-NP manifested robust heat generation capability ( $\Delta T = 40$  °C) and efficiently produced reactive oxygen species essential for PTT and PDT, respectively, without releasing SiNc from

the nanopaltform. By varying laser power density from  $0.3 \text{ W/cm}^2$  to  $1.3 \text{ W/cm}^2$  the therapeutic mechanism of SiNc-NP could be switched from PDT to combinatorial PDT-PTT treatment. *In vitro* and *in vivo* studies confirmed that phototherapy mediated by SiNc can efficiently destroy chemotherapy resistant ovarian cancer cells. Remarkably, solid tumors treated with a single dose of SiNc-NP combined with NIR irradiation were completely eradicated without cancer recurrence. Finally, the efficiency of SiNc-NP as an NIR imaging agent was confirmed by recording the strong fluorescence signal in the tumor, which was not photobleached during the phototherapeutic procedure.

KEYWORDS: naphthalocyanine, photothermal therapy, photodynamic therapy, near-infrared imaging, photostability, theranostic

### Table of contents graphic



## 1. Introduction

Theranostic nanomedicine, where therapeutic and imaging features are integrated within a single platform, offers the unique opportunity for concurrent diagnostic and treatment of cancer tumors.<sup>1</sup> Phototherapy is one of the promising non-invasive clinical approaches to eradicate cancer owing to its high efficiency and minimal side effects, which are achieved by selective illumination of the cancer site with light of an appropriate wavelength.<sup>2, 3</sup> When represented by photodynamic (PDT)<sup>2, 4</sup> or photothermal (PTT)<sup>3, 5, 6</sup> therapies, the phototherapy requires light and photoactive agents to generate reactive oxygen species (ROS) or heat, respectively. PDT selectively damages cancer tissues by ROS generated in the presence of molecular oxygen by light activation of a photoactive drug.<sup>2</sup> Unlike PDT, PTT does not require oxygen accessibility to damage targeted tissues and generates localized hyperthermia from absorbed light for destruction of hypoxic tumors.<sup>3, 5-7</sup> As both PDT and PTT act via different mechanisms, their combination into a single therapeutic modality provides a highly efficient approach to treat neoplastic tissues. The combinatorial phototherapy can be an efficient treatment of chemo- and radio- resistant cancer cells by involving cytotoxic mechanisms distinct from chemo- and radiotherapies.<sup>8</sup> The addition of imaging abilities to such a combinatorial modality also allows identification of microscopic cancer tumors for more precise and highly efficient treatment.<sup>1</sup> For clinically relevant use, ideal imaging, PDT and PTT agents should exhibit strong absorbance in the near-infrared (NIR) region, a transparency window for biological tissues, and could efficiently transfer the absorbed NIR optical energy into fluorescence, ROS and heat, respectively.<sup>9</sup> Moreover, fluorescence imaging in the “NIR optical window” holds much promise due to minimal tissue autofluorescence and light scattering.<sup>9</sup>

Recently, several multifunctional theranostic systems have been developed for achieving NIR fluorescence imaging and combinatorial phototherapeutic treatment of cancer.<sup>10-15</sup> The main approach for the construction of these systems is based on integration of separate imaging and therapeutic components into nanocarriers, which result in a more complex composition.<sup>10-15</sup> Application of several imaging and therapeutic agents can potentially increase side effects of the developed nanoplatform on healthy organs and raise its manufacturing cost. Furthermore, some of the developed systems could not be activated with a single light source due to the absorption mismatch of the PTT and PDT agents.<sup>11-15</sup> The sequential irradiation based on two lasers with different wavelengths prolongs the treatment time and requires precise alignment of the two light beams. It may also prevent the superior synergistic effect, which could be only achieved by simultaneously generating intracellular heat and toxic ROS in the intracellular environment. Moreover, a theranostic system prepared by integration of the therapeutic agents excitable at a single wavelength<sup>10</sup> must be carefully designed to attain the desired concentration ratio of encapsulated PDT and PTT agents and synchronize their release profiles after cellular internalization to achieve the required synergistic therapeutic effect. Consequently, the development of a simple, single agent-based theranostic nanoplatform that can provide both cancer imaging and a synergistic therapeutic effect is highly desired.

Due to the attractive photo-physical properties in the NIR range, some of the organic cyanine dyes can be potentially employed for the development of a single-agent based theranostic nanoplatform.<sup>16-19</sup> Thus, indocyanine green (ICG), the only FDA approved NIR imaging agent, also possesses some PDT and PTT properties.<sup>17, 20-22</sup> However, low photostability and a lack of cancer targeting, resulting in a fast photodegradation and quick clearance from the body

significantly hamper clinical application of ICG and the possibility to become a single theranostic agent *in vivo*.<sup>23-25</sup>

Among other NIR dyes, naphthalocyanine (Nc) with very strong absorption ( $\epsilon > 10^5 \text{ M}^{-1}\text{cm}^{-1}$ ) near 800 nm holds great promise for fluorescent imaging and combinatorial phototherapeutic treatment of deeply seated as well as pigmented tumors.<sup>26</sup> However, application of Nc as a theranostic agent, is substantially limited by poor water solubility and aggregation.<sup>26, 27</sup> Due to their planar structures, Nc molecules have a tendency to aggregate in aqueous medium through  $\pi$ - $\pi$  stacking and hydrophobic interactions, resulting in the self-quenching effect of their excited states.<sup>28</sup> Consequently, after exposure to NIR light, the aggregated Nc molecules in water solution can only dissipate the absorbed energy through nonradiative decay (heating), while fluorescence (imaging) and ROS production (PDT) are diminished.<sup>29, 30</sup> Recently, Mathew *et al.* constructed Nc-based lipoprotein nanocarriers with the ability to generate heat exclusively upon light irradiation.<sup>30</sup> In addition, Sigh *et al.* developed a theranostic nanomaterial for fluorescence imaging and PTT by integration of SiNc and IR780 dyes within mesoporous silica nanoparticles.<sup>31</sup> It is important to note that imaging ability of the developed theranostic nanoparticle was achieved by the incorporation of additional NIR dye, IR780, while Nc was used only as PTT agent.<sup>31</sup>

To explore PDT or imaging properties, Nc molecules have been modified with bulky organic ligands to provide the steric hindrance and lower intramolecular aggregation after their encapsulation into the interior of the nanomaterials.<sup>10, 32, 33</sup> For example, Jin *et al.* incorporated bis-substituted SiNc into the hydrophobic polymer dot matrix to enhance fluorescence emission of Nc.<sup>32</sup> Furthermore, Song *et al.* claimed that nanoparticles produced by modification of SiNc with oleate ligands following encapsulation into low-density lipoproteins can be potentially used

for fluorescence imaging and PDT, but these properties were not confirmed.<sup>33</sup> Recently, Gollavelli *et al.* developed a multicomponent theranostic system which consists of bis-substituted SiNc as a fluorescence and PDT agent, while graphene played a role of PTT agent.<sup>10</sup> A non-covalent approach, employed to immobilize photosensitizers onto water dispersible graphene, resulted in a significant decrease in the fluorescence signal and ROS generation of SiNc as a result of  $\pi$ - $\pi$  stacking interaction with graphene. To the best of our knowledge, no single NIR photoactive agent based on naphthalocyanine was reported which simultaneously (1) generates a strong NIR fluorescence signal inside of cancer cells required for image-guiding application, and (2) produces both toxic reactive oxygen species (PDT) and heat (PTT) for specific and efficient destruction of cancer cells with combinatorial phototherapy.

The work presented here addresses the development of an effective approach for transformation of naphthalocyanine into an effective single agent-based theranostic nanoplatform capable of concurrent NIR fluorescence imaging and combinatorial phototherapy. As shown in Figure 1, the designed structure of SiNc-loaded nanoplatform (SiNc-NP) is based on the encapsulation of substituted SiNc into the interior of a generation 5 polypropylenimine (PPI G5) dendrimer that is then surrounded with the biocompatible polyethylene glycol (PEG) polymer on the surface. The specific structure of PPI dendrimer, having a number of hydrophobic pockets,<sup>34</sup> offers the possibility to encapsulate and separate the SiNc molecules and thus decrease their aggregation, preserve imaging, PDT and PTT properties and enhance water solubility. Consequently, SiNc-NP with a hydrophobic naphthalocyanine within the PPIG5 dendrimer provide favorable properties for theranostic activity in terms of NIR absorption, PDT and PTT conversion efficiency, NIR fluorescence and photostability without the need for SiNc release.

## 2. Materials and methods

**Materials.** Silicon 2,3-naphthalocyanine dihydroxide (SiNcOH **1**) and silicon 2,3-naphthalocyanine bis(trihexylsilyloxy) (SiNc **2**) were purchased from Sigma-Aldrich (St. Louis, MO). Indocyanine green (ICG) was purchased from VWR Int. Polypropylenimine dendrimer generation 5 (PPIG5) was obtained from SyMO-Chem (Eindhoven, The Netherlands).  $\alpha$ -Succinimidylsuccinyl- $\omega$ -methoxy, polyoxyethylene (Methoxy-PEG-NHS, 2000 Da) was obtained from NOF Corporation (White Plains, NY). All other chemicals were of analytical grade and were purchased from VWR Int., Sigma-Aldrich and Fisher Scientific Inc.

### Preparation and Characterization of Theranostic Nanoplatform

**Encapsulation of SiNc into dendrimers.** Nc encapsulation was achieved by sonication of 10 mg of PPIG5 in methanol (0.6 mL) mixed with 10 mg of an appropriate naphthalocyanine (SiNcOH **1** or SiNc **2**) in THF (1.0 mL) for 15 min following by stirring at room temperature. After overnight stirring, organic solvents were evaporated and resulting solids were dissolved in water and purified using size exclusion chromatography (a 1 cm  $\times$  18 cm Sephadex G50 column). The dendrimer-based complexes of SiNcOH **1** and SiNc **2** will be further mentioned as SiNcOH-PPIG5 and SiNc-PPIG5, respectively. To determine drug loading efficiency for each individual naphthalocyanine, the obtained solutions were freeze-dried to remove water, followed by weighing of the obtained pellets and re-dissolving in THF. The amount of Nc encapsulated into the PPIG5 was quantified based on UV-visible absorption spectra of Nc-PPI G5 samples in THF, with a prominent Q-bands appearing at 767 nm and 772 nm for SiNcOH-PPIG5 and SiNc-PPIG5, respectively (UV-1800 spectrophotometer, Shimadzu, Carlsbad, CA). The standard curves were generated by measuring Nc absorption intensity at the above mentioned wavelengths in the standard samples containing different concentrations of SiNc. Nc loading efficiency is

expressed as the percentage of Nc weight encapsulated into PPIG5 over the weight of the Nc-PPIG5 complexes.

**Modification of SiNcOH-PPIG5 and SiNc-PPIG5 with PEG.** The previously published procedure was employed to modify the Nc-PPIG5 complexes with PEG.<sup>35</sup> Briefly, the NHS group of monofunctional 2 kDa PEG polymer (Methoxy-PEG-NHS) was reacted with primary amine on the surfaces of PPIG5 dendrimer in 50 mM PBS buffer (pH 7.6), at dendrimer to PEG molar ratio of 1:32. The concentration of amino groups available on the PPIG5 surface for PEGylation and the decrease in their concentration after the surface modification was determined by a modified spectrophotometric TNBSA assay.<sup>36</sup> The reaction was carried out under shaking at room temperature. After 12 h, the modified complexes were purified by using size exclusion chromatography (a 1 cm × 18 cm Sephadex G75 column) to yield stable in water SiNcOH-PPIG5-PEG and SiNc-PPIG5-PEG nanopatform which will be further mentioned as SiNcOH-NP and SiNc-NP, respectively.

**Absorption and Fluorescence Measurements.** Absorption and fluorescence spectra of SiNcOH-NP and SiNc-NP in PBS buffer and free SiNcOH 1 and SiNc 2 in THF were measured using a UV-1800 spectrophotometer (Shimadzu, Carlsbad, CA) and Cary Eclipse R3896 fluorescence spectrophotometer (Varian Inc., Mulgrave Victoria, Australia), respectively.

**Size and Zeta Potential Measurements.** The hydrodynamic size and zeta potential of the prepared complexes were measured by Malvern ZetaSizer NanoSeries (Malvern Instruments, UK) according to manufacturer's instructions. Samples were diluted with 50 mM PBS buffer (pH 7.4) to yield a final Nc concentration of ~1.0 µg/mL. The intensity of the He-Ne laser (633 nm) was measured at an angle of 173°. All measurements were performed at 25 °C after pre-equilibration for 2 min and each parameter was measured in triplicate.

**Singlet Oxygen  $^1\text{O}_2$  Measurements.**  $^1\text{O}_2$  production was evaluated by using Singlet Oxygen Sensor Green (SOSG) assay (Life Technologies, Grand Island, NY). SOSG in the presence of singlet oxygen emits a green fluorescence (excitation/emission max  $\sim 504/525$  nm). To the parallel wells of the 96 well opaque plate (Corning), 40  $\mu\text{l}$  of the 25  $\mu\text{M}$  stock solution of SOSG in methanol, 50  $\mu\text{L}$  of  $\text{H}_2\text{O}$ , and 10  $\mu\text{L}$  of either SiNcOH-PEG or SiNc-PEG (SiNc  $\sim 100$   $\mu\text{g}/\text{ml}$ ) in MilliQ water were added to give working concentrations of 10  $\mu\text{M}$  SOSG and 10  $\mu\text{g}/\text{ml}$  SiNc in a final volume of 100  $\mu\text{l}$  per well. Next, some wells were irradiated with light (785 nm, 0.3  $\text{W}/\text{cm}^2$ , 5 min) while the dark control was kept covered. Immediately, the samples were analyzed on Cary Eclipse R3896 fluorescence spectrophotometer (Varian Inc., Mulgrave Victoria, Australia) using an excitation of 504 nm and emission of 525 nm. All experiments were performed in triplicate.

**Temperature Evaluation Induced by Laser Irradiation:** A continuous wave (CW) 785 nm laser diode (Intense, North Brunswick, NJ, 0.3, 0.75 and 1.3  $\text{W}/\text{cm}^2$ ) operated with the laser diode driver (ThorLabs, Newton, NJ) was employed. To evaluate the laser induced temperature increase, 300  $\mu\text{L}$  of either SiNcOH-NP or SiNc-NP aqueous solutions (100  $\mu\text{g}/\text{ml}$ ) were added into the clear 0.5 mL vials, respectively. Then each vial was irradiated with the laser diode for 20 min, while the temperature was monitored with thermocouple thermometer (VWR Int.) at designated time intervals. In addition, 300  $\mu\text{L}$  of free SiNc 2 dissolved in THF (100  $\mu\text{g}/\text{ml}$ ) and 300  $\mu\text{L}$  of dionized water were irradiated at the same laser settings for temperature recording.

**Photostability.** To investigate photostability, absorption spectra of SiNc-NP and ICG aqueous solutions and free SiNc 2 in THF at  $\text{OD}_{770} = 1.2$  were recorded prior to and after 30 min irradiation with the laser diode (785 nm, 1.3  $\text{W}/\text{cm}^2$ ). Furthermore, light and fluorescence images of the studied solutions before and after irradiation were acquired with Li-COR Pearl Animal

Imaging System. Finally, the photothermal stability of both SiNc-NP and ICG was evaluated by exposing optically matched ( $OD_{770} = 0.5$ ) SiNc-NP and ICG water solutions to the laser diode (785 nm,  $1.3 \text{ W/cm}^2$ ) for 20 min. The temperature of the studied solutions was monitored with thermocouple thermometer (VWR Int.) at designated time intervals.

### **In Vitro Study**

Only SiNc-PEG was selected as potential theranostic agent for further *in vitro* and *in vivo* studies and will be referred as naphthalocyanine nanoplatform (SiNc-NP).

**Cell Culture.** The A2780/AD doxorubicin resistant human ovarian carcinoma cell line was obtained from T. C. Hamilton (Fox Chase Cancer Center, Philadelphia, PA). Cells were cultured in RPMI 1640 medium (Sigma, St. Louis, MO) supplemented with 10% fetal bovine serum (VWR, Visalia, CA) and 1.2 mL/100 mL penicillin–streptomycin (Sigma, St. Louis, MO). Cells were grown at 37 °C in a humidified atmosphere of 5%  $\text{CO}_2$  (v/v) in air. All experiments were performed on cells in the exponential growth phase and between passages 2 and 6.

**Cytotoxicity Study in Dark and under NIR light exposure.** The dark cellular cytotoxicity of SiNc-NP was assessed under subdued lighting using a modified Calcein AM cell viability assay (Fisher Scientific Inc.).<sup>35</sup> Cancer cells were seeded into two 96-well microtiter plates at the density of  $10 \times 10^3$  cells/well and allowed to grow for 24 h at 37 °C. Then the culture medium was discarded and the cells were treated for 12 h with 100  $\mu\text{L}$  of medium containing different concentrations (2.5, 5.0, 10.0, 25.0, 50.0, and 100.0  $\mu\text{g/mL}$ ) of SiNc in the dark. A2780/AD cells only in fresh medium were used as a control. After 12 h of treatment, the Nc-containing medium was then replaced with fresh medium. One of the tested plates was exposed to a NIR 785 nm laser diode at  $0.3 \text{ W/cm}^2$  for 10 min (Intense, North Brunswick, NJ). Next day, the cells were

rinsed with DPBS buffer and incubated for 1 h with 200  $\mu$ L of freshly prepared Calcein AM solution (10  $\mu$ M in DPBS buffer) in the dark. Fluorescence was measured using a multiwell plate reader (Synergy HT, BioTek Instruments, Winooski, VT) with a 485 nm excitation and a 528 nm emission filters. On the basis of these measurements, cellular viability was calculated for each concentration of the formulation tested. The relative cell viability (%) was expressed as a percentage relative to the untreated control cells. The 50% inhibitory concentration (IC<sub>50</sub>) was determined as the drug concentration that resulted in a 50% reduction in cell viability.

**Combinatorial Phototherapy.** All manipulations prior to light treatment were carried out under subdued lighting. A2780/AD cells were plated in T-25 cell culture flasks and grown to 80% of confluence. Subsequently, cells were incubated for 12 h with SiNc-NP (25  $\mu$ g/mL) dispersed in 6 mL of cell culture media. Cells loaded with the nanoplatform were washed with DPBS in order to remove loose SiNc-NP, detached by using 0.25% trypsin/EDTA and resuspended in cell culture media prior to counting. Subsequent to counting, a portion of the cell suspension containing  $2 \times 10^6$  cells was centrifuged at 1000 rpm for 5 min to form the cell pellet. The formed cell pellets were maintained in a constant volume of 0.25 mL of culture media in a standard 0.5 mL microcentrifuge tube before and during treatment. Samples were then positioned on a heating block at 37 °C at exposed to the laser diode (785 nm, 1.3 W/cm<sup>2</sup>, 10 min) and the temperature changes were measured in 30-s intervals by placing a fiber optic temperature probe (Neoptix Inc., QC, Canada) inside of the pellets. After light exposure, the cells were washed with DPBS buffer, resuspended in media and seeded in a 96-well plate at a density of  $10 \times 10^3$  cells/well and were cultured for another 24 h. Finally, the cell viability was assessed using a modified Calcein AM assay as described above. In addition, three following control groups were employed in the current study to evaluate efficacy of combinatorial phototherapy: (1) untreated

cells, (2) cells treated with SiNc-NP and SiNcOH-NP (25  $\mu\text{g}/\text{mL}$ ) under dark conditions, (3) untreated cells exposed to the laser diode (785 nm, 1.3  $\text{W}/\text{cm}^2$ , 10 min), (4) photodynamic therapy only (SiNc-NP exposed to 0.3  $\text{W}/\text{cm}^2$  light), and (5) photothermal therapy only (SiNcOH-NP exposed to 1.3  $\text{W}/\text{cm}^2$  light).

**ROS Measurements.** Intracellular ROS levels were determined by using 2',7'-dichlorodihydrofluorescein diacetate (DCFH-DA) assay as previously described.<sup>35, 37</sup> Briefly, A2780/AD cells were seeded in 96-well microtiter plates at a density of  $10 \times 10^3$  cells/well followed by incubation with medium containing SiNc-NP at SiNc concentration of 25  $\mu\text{g}/\text{mL}$  for 12 h. After incubation, the cells were rinsed with warm DPBS and 100  $\mu\text{L}$  of 10  $\mu\text{M}$  DCFH-DA was added under subdued light conditions 30 min prior to light treatment. The test samples were exposed to the 785 nm laser diode light at a power density of 1.3  $\text{W}/\text{cm}^2$  for 10 min. In parallel, SiNc-NP without light irradiation was used as a dark control in addition to the cell only as control. Cells only treated and non-treated with light showed the same ROS production and were considered as 100%. Fluorescence was measured using a multiwell plate reader with a 485 nm excitation and a 528 nm emission filters.

**Quantification of intracellular Nc content.** The absorption spectra were used to estimate the intracellular Nc content in A2780/AD cells after treatment with the developed nanoplatform. In a prior analysis, cells were plated in T-25 cell culture flask and grow to 80% of confluence. The SiNc-NP (25  $\mu\text{g}/\text{mL}$ ) was then added to the cells. After 12 h of incubation, the cells were washed three times with DPBS buffer, trypsinized and counted by using hemocytometer. Further,  $5 \times 10^6$  cells were lysed with 0.5 mL of 50 mM NaOH for 2 h on a shaker at room temperature. The cell lysate (100  $\mu\text{L}$ ) was mixed with 900  $\mu\text{L}$  THF to dissolve SiNc. The absorbance readings at 772 nm were performed using UV-1800 spectrophotometer (Shimadzu,

Carlsbad, CA). The amount of SiNc uptaken by A2780/AD cells was quantified based on the standard curves generated by measuring SiNc absorption intensity at 772 nm in the standard samples containing different concentrations of Nc. The net cellular uptake of the drug delivery systems is expressed as weight (pg) of SiNc per cell.

### **In Vivo Study**

**Tumor Transplantation.** Approval for the animal studies was obtained from the Oregon State University Institutional Animal Care and Use Committee (IACUC) and the experiments were all conducted in accordance with IACUC policies. A dual tumor animal model of human ovarian carcinoma xenografts was established as following. Human ovarian carcinoma A2780/AD resistant cells ( $5 \times 10^6$ ) suspended in RPMI 1640 cell culture media were subcutaneously injected into each flank of 6-week-old female athymic nu/nu mice purchased from the National Cancer Institute (NCI). The tumor size was measured with a digital caliper (VWR Int.), and the tumor volume was calculated as  $\text{width}^2 \times \text{length} \times 0.5$  for 25 days.

**Imaging and Phototherapy:** On post-implantation day 7, when the tumors reached a size of about  $40 \text{ mm}^3$ , the mice were imaged before the SiNc-NP injection using Li-COR Pearl Animal Imaging System with 800 nm channel. The mice were randomly distributed to one of three groups (five mice per group): (1) control (right tumor) and NIR laser (left tumor), (2) control (right tumor) and SiNc-NP (left tumor), and (3) control (right tumor) and SiNc-NP + NIR laser (left tumor). Next, the corresponding tumors underwent intratumoral injection of SiNc-NP (200  $\mu\text{g}/\text{mL}$ , 15  $\mu\text{L}$ ). Fluorescent images were obtained after the injection to determine the Nc location. At 6 h post-injection, the mice in the particular experimental groups underwent one-time phototherapy (continuous wave laser, 785 nm, 1.3  $\text{W}/\text{cm}^2$ , 10 min) under isoflurane anesthesia. After treatment, the mice were monitored daily. Fluorescence imaging, body weight

and tumor size were recorded for all mice during 25 days following treatment. In case where the tumors disappeared, the tumor volumes were recorded as “zero”. Mice were euthanized at the defined end point when tumor diameter reached 13 mm.

**Intratumoral Temperature Monitoring.** During the NIR irradiation, the temperature changes in tumor were measured in 30-s intervals by placing a fiber optic temperature probe (Neoptix Inc., QC, Canada) into a tumor through a thin (18-gauge) needle. The fiber optic probe was protected inside of needle shaft from light exposure to avoid temperature misreading.

**Immunohistochemistry (IHC).** Samples of control (untreated and NIR light only treated (785 nm, 1.3 W/cm<sup>2</sup>, 10 min) tumor, tumor treated with SiNc-NP (SiNc-NP dark) and tumor treated with SiNc-NP and NIR 1.3 W/cm<sup>2</sup> (SiNc-NP light) were harvested 24 h after treatment from nude mice and immediately fixed overnight in a 4% paraformaldehyde DPBS solution. The fixed tissues samples were dehydrated in ethanol, cleared in xylene and incubated in paraffin at 60 °C for 24 h followed by paraffin block embedding. Next, the formalin-fixed paraffin embedded tissues were sectioned at 5 μm using a Leica RM2255 microtome (Bannockburn, IL) and collected onto slides and finally incubated at 60 °C overnight. Then, the rehydrated slides underwent antigen retrieval according to the previously published method<sup>38</sup> by being microwaved for 5 min (4x) in a pH 6.0 citrate buffer. After the slides were cooled to room temperature and washed (3x) in Phosphate Buffered Saline (PBS) solution with the detergent Tween® 20 PBS 0.05% (PBST), the sections on each slide were blocked in 10% normal goat serum (NGS) (Vector Laboratories, Burlingame, CA) for 1 h. Next, the sections were incubated at 4 °C with the primary caspase-3 antibody (Cell Signaling Technology, Danvers, MA) prepared in NGS at a dilution of 1:350 in a dark humidified box overnight. The next day, the primary antibody was washed off (3x) in PBST and the secondary antibody was added in a 1:1000

dilution and allowed to incubate in the dark for 2 h at room temperature. After the secondary antibody was rinsed off (3x) in PBST, the slides were incubated with 4',6-diamidino-2-phenyl indole (DAPI) at a 1:5000 dilution for 10 min for nuclei visualization followed by wash in PBST(3x), dehydration in ethanol and clearance in xylene. Finally, slides were mounted using DPX mounting media and analyzed using a Carl Zeiss Axio Imager Z1 fluorescent microscope (Thornwood, NY) and AxioCam camera.

**Statistical Analysis.** Data were analyzed using descriptive statistics, single-factor analysis of variance (ANOVA), and presented as mean values  $\pm$  standard deviation (SD) from three to five independent measurements. The comparison among groups was performed by the independent sample student's t-test. The differences were considered significant at a level of  $P < 0.05$ .

### 3. Results and discussion

**Preparation and Characterization of SiNc-NPs.** To develop an effective Nc-based theranostic nanoplatform with both phototherapeutic and imaging functions, silicon naphthalocyanines were selected for this study (Figure 1A). One advantage that silicon naphthalocyanines possess is the presence of two axial hydroxyl groups at the silicon center, which provide an opportunity to tune naphthalocyanines chemical and photo-physical properties via hydroxyl group functionalization.<sup>39, 40</sup> Silicon 2,3-naphthalocyanine bis(trihexylsilyloxy) (SiNc **2**) was preferably chosen due to the presence of two bulky linkers, trihexylsilyloxy, at the silicon center, which provide the steric hindrance to Nc molecules and reduce intermolecular aggregation via  $\pi$ - $\pi$  stacking.<sup>41</sup> Our previous work also demonstrated that the appropriate hydrophobic substituents in phthalocyanine can improve its solubility in organic solvents, thus enhancing its loading efficiency into the hydrophobic interior of the dendrimer.<sup>35</sup> In addition to the substituted SiNc **2**, parent silicon naphthalocyanine, a silicon 2,3-naphthalocyanine

dihydroxide (SiNcOH **1**), carrying two unsubstituted hydroxyl groups (Figure 1A), was selected to evaluate the influence of the linkers on theranostic properties of the prepared nanomedicine platform.

To preserve the photo-physical properties and attain aqueous solubility of the above mentioned silicon naphthalocyanines, the co-solvent evaporation method was employed for an efficient encapsulation of Nc molecules within the hydrophobic interior of amine terminated PPI dendrimers. PPI dendrimers have a number of hydrophobic compartments that enable the possibility of encapsulation and separation of the Nc molecules, and hence reduce their aggregation and enhance aqueous solubility (Figure 1B).<sup>42-44</sup> The presence of primary amine groups on the dendrimer surface provides an opportunity for functionalization of the prepared complexes with different molecules, including biocompatible PEG. In addition, the specific structure of the PPI dendrimer offers uniform size and optical transparency for theranostic applications.<sup>45</sup>

To achieve optimal Nc encapsulation into the dendrimer interior, parent naphthalocyanine (SiNcOH **1**) and its substituted derivative (SiNc **2**) were solubilized in THF and mixed with the methanol solution of the PPI dendrimers of different generations (Figure 1B). After overnight stirring at room temperature, organic solvents were evaporated and the resultant complexes were easily dissolved in water followed by purification via size exclusion chromatography. The resulting SiNc-PPI complexes were green in color indicating the encapsulation of the dye and solubility in water owing to the PPI dendrimers (Figure 1B). It must be noted that only the PPI dendrimer of generation 5 (G5), compared to lower generations of PPI dendrimers (G3 and G4), exhibited sufficient loading efficiency for naphthalocyanines. This is attributed to the fact that dendrimer molecules of higher generations are characterized by larger hydrophobic pocket

volume and, therefore, can encapsulate more SiNc molecules.<sup>34</sup> The Nc loading efficiency of 16 % w/w was detected for SiNc **2** in PPIG5 whereas this value was only 6 % w/w for SiNcOH **1**. The lower encapsulation efficiency for unsubstituted SiNc is related to its reduced solubility in organic solvents (e.g. THF), which were employed for the co-solvent evaporation method. This problem was overcome in the case of SiNc **2** by the introduction of two hydrophobic substituents. A similar issue was previously reported by us for encapsulation of unsubstituted phthalocyanine molecules into the dendrimer interior.<sup>35</sup>

A steric stability and solubility in physiological solutions is essential for nanomedicine platforms to provide the required theranostic properties and avoid side effects on the human body.<sup>1, 27, 41</sup> To improve stability and biocompatibility, SiNc-PPIG5 complexes were modified with 2 kDa PEG polymer (Figure 1B), carrying an amine reactive NHS ester. The modification was carried out by the coupling of linear Methoxy-PEG-NHS to the amino groups on the dendrimer surface at a PPIG5/PEG ratio of 1:32 giving the final water-soluble naphthalocyanine-loaded nanoplatform (SiNc-NP). The decrease in the number of surface amine groups and presence of the PEG layer on SiNc-NPs led to the much lower surface charge (SiNcOH-NPs,  $+6.2 \pm 3.2$  mV; and SiNc-NPs,  $+1.2 \pm 3.7$  mV) compared to non-modified SiNc-PPIG5 complexes (SiNcOH-PPIG5,  $+43.3 \pm 4.1$  mV; and SiNc-PPIG5,  $+42.1 \pm 3.5$  mV). The decrease in the concentration of primary amines on the periphery of dendrimer after a modification with PEG was additionally confirmed by the TNBSA assay. The nearly neutral surface charge, as in the case of the PEG-modified SiNc-NPs, will reduce the interaction of the delivery system with the blood serum proteins and macrophages during systemic circulation and decrease its toxicity related to the cellular membrane damage effect.<sup>6, 36</sup> In addition to the prolonged blood circulation time and reduced severe side effects on healthy organs, PEGylation of nanocarriers promotes a

high degree of drug accumulation within the target tumor via passive mechanisms of enhanced permeation and retention (EPR).<sup>46</sup> According to the size measurement, the hydrodynamic diameter of the SiNc-NP was evaluated to be  $149.2 \pm 0.2$  nm (Figure S1). Thus, the final nanocarriers have a hydrodynamic size within the desired range of 10-200 nm to prevent elimination by the kidneys ( $>10$  nm) and enhance tumor-targeted delivery via EPR effect ( $<200$  nm).

**Photo-Physical Properties of SiNc-NPs.** The fundamental feature for effective photoactive theranostic agents would be a strong absorption in the NIR region of the spectrum to promote efficient transmission of light energy to the deep-seated cancer tumors, which can be further converted into fluorescence emission, heat and ROS.<sup>47</sup> Naphthalocyanines including SiNc demonstrate the highly desired absorption in the NIR optical window for effective fluorescence imaging, photodynamic and photothermal therapies.<sup>28</sup> Hence, spectroscopic properties of the developed, water soluble SiNcOH-NP and SiNc-NP were evaluated. As shown in Figure 2A, the substituted SiNc 2 entrapped in the dendrimer-based nanocarrier (SiNc-NP) exhibited a strong NIR absorption in water with a relatively narrow absorbance peak at 782 nm (black curve) which was red-shifted by  $\sim 10$  nm from the Q-band maximum at 772 nm of monomeric non-encapsulated SiNc 2 dissolved in THF (blue curve). The detected bathochromic shift indicates formation of J-aggregates, stable fluorescent structures, as could be expected for silicon naphthalocyanines featuring two axial substituents.<sup>48</sup> On the contrary, un-substituted SiNcOH 1 loaded into PPIG5 (SiNcOH-NP) exhibited H-type aggregation in an aqueous solution, which is characterized by non-fluorescent structures and a broad absorption peak with a hypsochromic shift of  $\sim 30$  nm (red curve) from the Q-band maximum at 767 nm of monomeric SiNcOH 1 dissolved in THF (Figure 2A, green curve). It was previously indicated that naphthalocyanines,

which lack axial ligands, tend to form H-aggregates with concurrent loss of PDT and imaging properties.<sup>48</sup> Thus, the detected intense absorption of SiNc 2 complexes in the NIR region is within the NIR optical window (~750-900 nm) required for efficient imaging and phototherapy via both PDT and PTT mechanisms.<sup>9, 49</sup>

In the development of an effective naphthalocyanine-based theranostic agent, strong NIR absorption is required in addition to distinct fluorescence emission. However, extensive aggregation of naphthalocyanines in aqueous media due to large  $\pi$ - $\pi$  conjugated systems appears to be a major factor in the quenching of their excited state, which reduces their imaging and PDT efficiency.<sup>28</sup> Upon excitation with NIR light, only SiNc-NP complexes in aqueous media showed distinctive fluorescence emission at 820 nm (Figure 2B, black curve), which is related to the formation of fluorescent J-aggregates.<sup>48</sup> Almost no detectable fluorescence was observed for SiNcOH-NP (Figure 2B, red curve), which appears to be non-fluorescent H-type aggregates.<sup>48, 50</sup> In addition, the intense fluorescence signals of SiNc-NP complex dissolved in water have been recorded by Li-COR Pearl Animal Imaging System specifically designed for *in vivo* imaging in the NIR spectral region (Figure 2B, insets). Due to the presence of the emission peak at 820 nm for SiNc-NP, the fluorescence signal was detected with an 800 nm channel of the imaging system, which avoids tissue autofluorescence and light scattering. The obtained data revealed that encapsulation of substituted SiNc 2 within the hydrophobic interior of PPI G5 dendrimers decreases Nc aggregation and preserves fluorescence intensity after dispersion of nanocarriers in water solution. Intense absorption and fluorescence of SiNc-NP within the NIR therapeutic optical window provides a significant potential for application in fluorescence bioimaging.<sup>9</sup>

**PDT and PPT Properties of SiNc-NPs.** To confirm the potential of the developed SiNc-NP for both PDT and PTT, the ROS production and heat generation followed by NIR light

irradiation were evaluated. SiNc as a PDT agent within the developed nanoplatform is expected to produce toxic ROS to kill cancer cells, particularly singlet oxygen ( $^1\text{O}_2$ ). Thus,  $^1\text{O}_2$  generation was measured using the SOSG assay, which is exclusively selective toward  $^1\text{O}_2$  and not to other reactive oxygen species.<sup>51</sup> SiNcOH and SiNc were irradiated with a portable 785 nm laser diode of low power density ( $0.3 \text{ W/cm}^2$ ) for 5 min. Remarkably, SiNc-NP showed a 124% increase in  $^1\text{O}_2$  production immediately after light exposure when compared to the controls (Figure 3A, black bars). In contrast, the increase of  $^1\text{O}_2$  generated by SiNcOH-NP was only 7.8% under the same conditions (Figure 3A, red bars). These results indicate minimal PDT ability for unsubstituted SiNcOH, which is related to its intense aggregation within the nanoplatform and quenching of the excited state.<sup>41</sup> On the other hand, SiNc 2 with axial substituents within the developed nanoplatform showed distinctive singlet oxygen production and thus high potential for effective PDT.

Rising and maintaining an elevated temperature at the cancer site is one of the key factors for an efficient photothermal therapy as the protein denaturation, disruption of the cellular membrane and ablation of tumor tissues occur at temperatures  $\geq 40\text{-}43 \text{ }^\circ\text{C}$ .<sup>52</sup> After exposure to NIR light, silicon naphthalocyanines are expected to increase the local temperature significantly enough to cause irreversible photothermal damage to the tumor cells. To verify photothermal properties of silicon naphthalocyanines encapsulated within the dendrimer nanoplatform upon activation with NIR light, both SiNcOH-NP and SiNc-NP were exposed to the 785 nm NIR laser at the power density of  $1.3 \text{ W/cm}^2$ , and temperature changes at 2 min time intervals for 20 min were recorded. The temperature profiles of both samples (SiNcOH-NP and SiNc-NP) at the same concentration ( $100 \text{ }\mu\text{g/mL}$ ) had a quick rising phase during the first 5 min followed by a sustained plateau at  $64 \text{ }^\circ\text{C}$ . Under the same experimental conditions, the water control showed a

temperature increase of only 1.0 °C, clear evidence that only SiNc-NP can efficiently convert absorbed light energies into heat and raise the temperature of the surrounding medium. It is worth mentioning that encapsulation of SiNc into the dendrimer interior and J-aggregates formation significantly improves its photothermal properties in comparison to non-encapsulated monomeric SiNc. As indicated in Figure 3B, free monomeric SiNc **2** dissolved in THF (blue curve) was able to increase the temperature of the solution to only 40 °C, while the temperature of the SiNc-NP solution was raised to 64 °C under the same experimental conditions.

The further experiments also revealed that when the power density of a laser beam was lowered to 0.3 W/cm<sup>2</sup>, no rise in temperature was detected for SiNc-NP (Figure 3C). Thus, by varying laser power density from 0.3 W/cm<sup>2</sup> (Figure 3C, red curve) to 1.3 W/cm<sup>2</sup> (Figure 3C, blue curve) the therapeutic application of SiNc-NP could be tuned from PDT to combinatorial PDT-PTT treatment, and *vice versa*. In addition, by changing the laser power the desired temperature outcome can be adjusted, providing the possibility for controlled hyperthermia. We demonstrated that increasing the power density of a laser to 0.75 W/cm<sup>2</sup>, SiNc-NP demonstrated a temperature increase with a continuous plateau at 42-43 °C over 20 min (Figure 3C, black curve). The temperature of the same solution was raised to 64 °C at the higher power density of a laser (1.3 W/cm<sup>2</sup>) (Figure 3C, blue curve). The obtained data suggest that the single agent SiNc-NP has excellent potential to become a nanoplatform with double tunable therapeutic anticancer properties, such as PDT and PTT.

**Photostability.** The enhanced photostability of an NIR agent is crucial for phototherapy, especially via a mild hyperthermic mechanism, where a prolonged elevated temperature is required.<sup>29, 30</sup> As for an imaging agent, photobleaching could be misinterpreted as a lack of fluorescence contrast, which would give false negative results. Considering that Nc

photodegradation can substantially affect theranostic properties of the developed nanomedicine platform, the photostability of SiNc-NP was evaluated and compared to ICG, which is widely used as an NIR agent for imaging and photothermal therapeutic formulations.<sup>53-56</sup> According to our data, the NIR irradiation of the water solution of SiNc-NP with a 785 nm diode laser (1.3 W/cm<sup>2</sup>) for 30 min did not cause a noticeable decrease in either absorption or fluorescence intensity of SiNc (Figure 4A), implying photostability of the SiNc-NP. As shown in Figure 4A (insets), SiNc-NP retained both the green color and fluorescence of naphthalocyanine after 30 min of laser irradiation. In contrast, ICG exposed to the same laser power demonstrated a drastic decrease in absorbance and fluorescence, and the blue color of the solution was completely bleached, suggesting almost full decomposition of ICG (Figure 4B). Remarkably, that non-encapsulated monomeric SiNc 2 also demonstrates unusually high photostability in comparison to ICG dye. Thus, only a 10% decrease in absorption intensity was detected for free monomeric SiNc 2 dissolved in THF after 30 min irradiation with laser light at a power density of 1.3 W/cm<sup>2</sup> (Figure S2), while an 82% decrease was observed for ICG under exposure to the same light (Figure 4B). It was previously reported that silicon naphthalocyanines with axial substituents exhibit greater photostability compared to unsubstituted Zn- and Al- naphthalocyanines.<sup>28</sup>

These observations are consistent with variances in photothermal efficiency of SiNc-NP and ICG, where ICG was unable to maintain an elevated temperature upon irradiation. Figure 4C shows a temporal photothermal profile measured in uncapped Eppendorf tubes, where the concentrations of SiNc 2 and ICG were adjusted so that optical densities at 770 nm were identical ( $OD_{770} = 0.5$ ) in the two samples for comparison. The solution of ICG reached a maximum temperature of 52 °C after 7 min of irradiation (Figure 4C, red curve) prior to the gradual decrease in the temperature reaching 38 °C after 20 min. The temperature declination

after initial heating is attributable to the degradation of ICG under the condition with intense laser excitation and localized heat generation.<sup>29</sup> In contrast, our nanomedicine platform where SiNc is encapsulated within the PPIG5-PEG system demonstrated superior photothermal stability under the same experimental conditions (Figure 4C, blue curve). The comparison with ICG indicates that SiNc **2** molecules encapsulated in the dendrimer interior are highly stable optically as well as thermally, being a promising alternative to the FDA-approved ICG for the theranostic applications requiring prolonged or intense light illumination.

***In vitro* study.** The promising photo-physical properties of the developed formulation prompted us to explore the efficiency of SiNc-NP as a theranostic nanoplatform both *in vitro* and *in vivo*. To evaluate the ability of the nanoplatform to treat chemotherapy resistant cancer, the doxorubicin resistant A2780/AD ovarian cancer cells were incubated with increasing concentrations of SiNc-NP (2.5 - 100  $\mu\text{g}/\text{mL}$ ) for 24 h following 10 min exposure to NIR light (785 nm, 0.3  $\text{W}/\text{cm}^2$ ) and cell viability was assessed using Calcein AM assay (Figure 5A). The laser power density of 0.3  $\text{W}/\text{cm}^2$  was specifically chosen for this experiment based on our solution studies (Figure 3 A and C), to evaluate only the photodynamic effect of SiNc-NP. After treatment, cells were cultured for 24 h in growth medium prior to viability measurements. Under dark conditions (no exposure to NIR light), toxicity of the SiNc-NP complex at the studied concentrations was minimal, whereas significant cell death (up to 62%) was detected upon the photoirradiation of the treated cells (Figure 5A). Minimal toxicity of phototherapeutic agents in the absence of NIR irradiation (dark cytotoxicity) is one of the main requirements for an efficient and safe phototherapy and fluorescence imaging.<sup>57, 58</sup> At the same time, activation of the cytotoxic function of the photoactive drug by targeted, locally applied light provides an opportunity for selective cancer treatment. Figure 5A demonstrates that cancer cell viability at

constant NIR light decreased as SiNc **2** concentration increased and 50% of the cell death ( $IC_{50}$ ) was detected at the concentration of 25  $\mu\text{g}/\text{mL}$ . Our results suggest that if needed, the developed nanoplatform can be employed for cancer cell treatment specifically via PDT mechanism by tuning power density of a laser light.

To evaluate efficacy of combinatorial phototherapy (PDT and PTT) generated by the developed nanoplatform, the A2780/AD cell pellets containing  $\sim 2,000,000$  cells were treated with SiNc-NP at the concentration of 25  $\mu\text{g}/\text{mL}$  ( $IC_{50}$  for PDT treatment) followed by irradiation with a laser diode of higher power density ( $1.3 \text{ W}/\text{cm}^2$ ) for 10 min. We revealed the superior efficacy of the combinatorial phototherapy mediated by SiNc-NP on doxorubicin-resistant ovarian carcinoma cells (A2780/AD) with more than 99% cancer cells death (Fig. 5B, yellow bar), in comparison to PDT (50% cells death, SiNc-NP +  $0.3 \text{ W}/\text{cm}^2$  light, cyan bar) and PTT (87% cell death, SiNcOH-NP +  $1.3 \text{ W}/\text{cm}^2$  light, magenta bar) alone. Notably, the toxicity of the nanoplatform was insignificant under dark conditions (no laser irradiation), indicating safety and specificity of the combinatorial phototherapy (Fig. 5B, red and green bars). The employed power density of light ( $1.3 \text{ W}/\text{cm}^2$ ) appears to be safe without causing A2780/AD cells death after irradiation with the laser diode for 10 min (Figure 5B, blue bar). The detected efficiency of the combinatorial phototherapy for treatment of chemotherapy resistant A2780/AD cancer cells cannot be achieved with doxorubicin concentrations as high as 250  $\mu\text{g}/\text{mL}$  (Figure S3). However, this data is in good agreement with our previous reports, which indicate the sensitivity of doxorubicin resistant A2780/AD cancer cells to PDT and hyperthermia.<sup>6, 35</sup> Therefore, the developed combinatorial phototherapy could be an efficient approach for intraoperative treatment of multidrug resistant cancer cells.

To confirm that both PDT and PTT mechanisms are activated under exposure of SiNc-NP-treated cancer cells to 785 nm laser light of  $1.3 \text{ W/cm}^2$  power density, intracellular ROS and temperature measurements have been performed. As both ROS and temperature generation efficiency strongly depend on the amount of photoactive agent internalized by cancer cells,<sup>57</sup> the amount of intracellular SiNc was additionally quantified under these experimental conditions by using absorption spectroscopy. It was revealed that A2780/AD cancer cells efficiently uptake the prepared nanoplatfrom yielding an intracellular SiNc concentration of approximately 9.6 pg/cell.

After exposure of the cancer cells with the above mentioned SiNc loading to NIR light ( $1.3 \text{ W/cm}^2$ ), the maximum achieved temperature of cell pellets was as high as  $52 \text{ }^\circ\text{C}$  (Figure 5C, black curve), whereas temperature change for non-transfected cells was less than  $1 \text{ }^\circ\text{C}$  (Figure 5C, red curve). An example of temperature profiles of measured cell pellets are represented in Figure 5C. Thus, with a starting temperature of  $34 \text{ }^\circ\text{C}$ , the SiNc-NP loaded A2780/AD cells exhibit rapid heating upon exposure to NIR light, crossing  $43.5 \text{ }^\circ\text{C}$  in 1 min and reaching  $52 \text{ }^\circ\text{C}$  in 6.5 min. The achieved cellular temperature can be maintained during the required periods of time in the presence of NIR light. However, switching off the laser resulted in the rapid cooling of cells to  $37 \text{ }^\circ\text{C}$  in 3 min.

Intracellular generation of cytotoxic ROS by SiNc upon light activation would confirm the activation of a PDT mechanism.<sup>2, 59</sup> Therefore, the intracellular ROS generation in A2780/AD cells treated with SiNc-NP and irradiated with NIR laser light ( $1.3 \text{ W/cm}^2$ ) was evaluated by DCFH-DA assay and compared to the ROS level in the following controls: (a) non-treated cells, (b) cells treated with SiNc-NP under dark conditions, and (c) cells exposed to light only (Figure 5D). The control samples demonstrated a similar ROS level, suggesting that the detected increase in ROS generation can be specifically attributed to the photodynamic effect of the

developed nanoplatform in the presence of light. As seen in Figure 5D, cells exposed to SiNc-NP and then subsequently irradiated with the NIR diode laser light for 5 min demonstrated a 5.8 fold elevation in general intracellular ROS level as compared to the controls.

The above data clearly indicate that our nanoplatform can only be activated for cancer treatment in the presence of NIR light; otherwise, the SiNc-NP nanoplatform is not toxic under dark conditions. Moreover, the therapeutic mechanism can be switched from PDT only ( $0.3 \text{ W/cm}^2$ ) to the combinatorial phototherapy ( $1.3 \text{ W/cm}^2$ ) by changing the laser power.

Efficacy of the different anticancer agents, including photoactive drugs, encapsulated into nanoparticles, strongly depends on drug release from the carriers. Notably, the SiNc molecules encapsulated in the developed nanoplatform do not have to be released in the cancer cells to cause the phototherapy effect. To prove this point, the SiNc release profile of the developed formulation has been evaluated in PBS at pH 5.5 containing 10 mM of reduced glutathione, mimicking intracellular (acidic and reduced) conditions with and without laser light irradiation (20 min, 785 nm,  $1.3 \text{ W/cm}^2$ ) (Figure S4). The obtained results revealed that drug release was minimal (less than 2%) under studied conditions including NIR light irradiation. The observed result is in a good agreement with our recently published work,<sup>35</sup> where the PDT effect was observed with the phthalocyanine-based theranostic platform without intracellular release.

Moreover, a critical feature for an efficient theranostic system is the ability to prevent leaching of photoactive agents from the nanocarriers in systemic circulation and, thus, minimize side effects and maximize delivery of the active component to the targeted tumors via EPR effect.<sup>46</sup> It was also demonstrated that the amount of SiNc released from the dendrimer in PBS buffer at pH 7.4 was less than 2%. According to these data, it can be assumed that the encapsulated SiNc molecules are not capable of escaping from the dendrimer-based carrier in the

blood stream and an intracellular environment due to their highly hydrophobic nature, and therefore cannot directly cause toxicity.<sup>35</sup>

***In Vivo* Biomaging and Therapeutic Efficacy of SiNc-NP.** After the successful *in vitro* results, we performed *in vivo* studies to evaluate NIR imaging ability and phototherapeutic efficacy of the developed theranostic nanoplatform. For *in vivo* experiments, A2780/AD ovarian cancer cells were subcutaneously transplanted into both the left and right flanks of nude mice. When the tumors volume reached 40 mm<sup>3</sup>, 15  $\mu$ L of SiNc-NP (SiNc 200  $\mu$ g/mL) was introduced to the left tumor region, while the right non-injected tumor was used as a control (Figure 6A and B). The efficiency of SiNc-NP as NIR imaging agent was confirmed by recording the strong fluorescence signal in the tumor area with 800 nm channel of Li-COR Pearl Animal Imaging System (Figure 6B), specifically designed for *in vivo* imaging in the NIR spectral region. No fluorescence signal was detected in the mouse before the SiNc-NP injection (Figure 6B), revealing that the recorded signal is not related to tissue autofluorescence. Importantly, the fluorescence signal was not decreased after exposure of the tumor area to a 785 nm laser at a power density of 1.3 W/cm<sup>2</sup> for 10 min (Figure 6C). This data further confirmed superior *in vivo* photostability of SiNc encapsulated in the developed nanoplatform, which is an essential feature for application in phototherapy and accurate bioimaging, image-guided surgery or intraoperative phototherapy, which requires prolonged exposure of the photoactive agents to laser light.<sup>60</sup>

To evaluate anticancer efficacy of the combinatorial phototherapy *in vivo*, tumors treated with SiNc-NP were exposed for 10 min to a 785 nm laser at a power density of 1.3 W/cm<sup>2</sup>. Under irradiation, the intratumoral temperature increased rapidly from 36.6 °C to 41 °C within 1 min, reaching a 43 °C plateau after 4 min (Figure 7A, black curve). In comparison, the

temperature of the tumor without SiNc-NP treatment had almost no changes under the same 785 nm irradiation conditions (Figure 7A, red curve). It is remarkably that solid tumors treated with a single dose of SiNc-NP combined with 10 min of light irradiation shrank gradually and were completely eradicated from the mice on the 11th day after treatment (Figure 7B, green curve). Importantly, the treated tumors did not regrow during 25 days before the mice were euthanized (Figure 7B, green curve). In contrast, the untreated tumors on the right flanks grew rapidly and the mice were euthanized on 25<sup>th</sup> day after treatment when tumor volume reached  $\sim 1000 \text{ mm}^3$  (Figure 6 and 7B, black curve). In addition, neither laser irradiation at the used power density nor only SiNc-NP injection could affect the tumor growth (Figure 7B, red and blue curves).

For apoptosis evaluation after combinatorial PDT+PTT treatment of ovarian cancer tumor using SiNc-NP, a cleaved caspase-3 antibody was used as an apoptotic marker for IHC. Among the caspases that have been studied in humans, proteolytically activated caspase-3 has shown the best correlation with cellular apoptosis.<sup>61</sup> After cellular staining with a cleaved caspase-3 antibody, the control and the SiNc-NP treated light and dark tissue samples were fluorescently imaged. Tumor tissue samples after phototherapy treatment clearly showed a dramatic increase in apoptotic cells compared to control (Fig. 8). When treated with SiNc-NP in the dark, no noticeable change was observed when compared to the non-treated control samples (Fig. 8B).

It should be noted that despite the strong anticancer effect of the combinatorial phototherapy, the body weights of the mice increased continuously during the testing period, indicating that there were no side effects that caused weight loss (Figure S5). Finally, not even slight skin burn was noticed after irradiating the SiNc-NP-free tumors for 15 min suggesting that used in this experiment 785 nm laser light at a power density  $1.3 \text{ W/cm}^2$  is safe for phototherapy making the

application for SiNc even more attractive. A previous report indicated that a 670 nm laser irradiation caused hemorrhaging on the treated area of the mouse body.<sup>62</sup>

#### 4. Conclusion

In summary, we reported a simple and effective approach for constructing a novel single-agent based theranostic nanoplatform for cancer imaging and treatment. The presented results indicate that only substituted naphthalocyanines can be efficiently loaded into the PPIG5 dendrimer interior. The developed encapsulation strategy offers a possibility to separate the SiNc molecules and thus decrease their aggregation, preserve NIR fluorescence signal, stabilize its PDT and PTT properties and enhance water solubility. The developed nanoplatform is characterized by superior photo- and thermal stabilities, which are essential for efficient clinical applications. Furthermore, SiNc-NP exhibits minimal dark cytotoxicity and remarkable combinatorial phototherapeutic effects on chemotherapy resistant ovarian cancer *in vitro* and *in vivo*, by conferring its cytotoxic effects through the high production of ROS and heat without releasing the photoactive agent from the nanoplatform. By varying laser power density the therapeutic mechanism of SiNc-NP could be switched from PDT to combinatorial PDT-PTT treatment and *vice versa*. Finally, the potential of SiNc-NP as NIR imaging agent was confirmed by recording the strong fluorescence signal in the tumor area, which was not compromised during phototherapeutic procedure. We anticipate that the developed theranostic nanoplatform can be potentially applied for NIR fluorescence image-guided surgery and intraoperative combinatorial treatment of ovarian cancer.

#### Conflict of Interests

The authors declare no competing financial interest.

## Supplementary Material

Figures S1 – S5: Size distribution of SiNc-NP measured by dynamic light scattering (Figure S1); absorption spectra of free SiNc **2** in THF before and after irradiation with the 785 nm laser diode for 30 min (Figure S2); *in vitro* cytotoxicity of free DOX against A2780/AD human ovarian cancer cells (Figure S3); the release profiles of SiNc from SiNc-NP under various conditions (Figure S4); body weight curves of the mice with or without treatment (Figure S5). This material is available at <http://www.thno.org/>.

## Acknowledgement

This work was supported in part by funding provided by the Medical Research Foundation of Oregon, PhRMA Foundation and the College of Pharmacy at Oregon State University.

## References

1. M. S. Muthu, D. T. Leong, L. Mei and S. S. Feng, *Theranostics*, 2014, 4, 660-677.
2. D. E. Dolmans, D. Fukumura and R. K. Jain, *Nat. Rev. Cancer*, 2003, 3, 380-387.
3. H. W. Huang and C. T. Liauh, *J. Med. Biol. Eng.*, 2012, 32, 1-10.
4. N. L. Oleinick, R. L. Morris and T. Belichenko, *Photochem. Photobiol. Sci.*, 2002, 1, 1-21.
5. N. H. Levi-Polyachenko and J. H. Stewart, *Open Nanomedicine J.*, 2011, 3, 24-37.
6. O. Taratula, R. K. Dani, C. Schumann, H. Xu, A. Wang, H. Song, P. Dhagat and O. Taratula, *Int. J. Pharmaceut.*, 2013, 458, 169-180.
7. S. Yanase, J. Nomura, Y. Matsumura, H. Kato and T. Tagawa, *Photodiagn. Photodyn.*, 2012, 9, 369-375.
8. S. Vinogradov and X. Wei, *Nanomedicine-UK*, 2012, 7, 597-615.
9. V. J. Pansare, S. Hejazi, W. J. Faenza and R. K. Prud'homme, *Chem. Mater.*, 2012, 24, 812-827.
10. G. Gollavelli and Y. C. Ling, *Biomaterials*, 2014, 35, 4499-4507.
11. M. Guo, H. Mao, Y. Li, A. Zhu, H. He, H. Yang, Y. Wang, X. Tian, C. Ge, Q. Peng, X. Wang, X. Yang, X. Chen, G. Liu and H. Chen, *Biomaterials*, 2014, Epub ahead of print.
12. Y. H. Wang, H. G. Wang, D. P. Liu, S. Y. Song, X. Wang and H. J. Zhang, *Biomaterials*, 2013, 34, 7715-7724.
13. A. Sahu, W. I. Choi, J. H. Lee and G. Tae, *Biomaterials*, 2013, 34, 6239-6248.

14. J. Lin, S. J. Wang, P. Huang, Z. Wang, S. H. Chen, G. Niu, W. W. Li, J. He, D. X. Cui, G. M. Lu, X. Y. Chen and Z. H. Nie, *ACS Nano*, 2013, 7, 5320-5329.
15. J. Y. Kim, W. I. Choi, M. Kim and G. Tae, *J. Control. Release*, 2013, 171, 113-121.
16. S. L. Luo, E. L. Zhang, Y. P. Su, T. M. Cheng and C. M. Shi, *Biomaterials*, 2011, 32, 7127-7138.
17. L. Wu, S. T. Fang, S. Shi, J. Z. Deng, B. Liu and L. T. Cai, *Biomacromolecules*, 2013, 14, 3027-3033.
18. C. L. Peng, Y. H. Shih, P. C. Lee, T. M. H. Hsieh, T. Y. Luo and M. J. Shieh, *ACS Nano*, 2011, 5, 5594-5607.
19. W. R. Chen, R. L. Adams, A. K. Higgins, K. E. Bartels and R. E. Nordquist, *Cancer Lett.*, 1996, 98, 169-173.
20. V. L. Dzurinko, A. S. Gurwood and J. R. Price, *Optometry*, 2004, 75, 743-755.
21. M. L. J. Landsman, G. Kwant, G. A. Mook and W. G. Zijlstra, *J. Appl. Physiol.*, 1976, 40, 575-583.
22. E. Crescenzi, L. Varriale, M. Iovino, A. Chiaviello, B. M. Veneziani and G. Palumbo, *Mol. Cancer Ther.*, 2004, 3, 537-544.
23. V. Saxena, M. Sadoqi and J. Shao, *J. Pharm. Sci.*, 2003, 92, 2090-2097.
24. T. Desmettre, J. M. Devoisselle and S. Mordon, *Surv. Ophthalmol.*, 2000, 45, 15-27.
25. S. Mordon, J. M. Devoisselle, S. Soulie-Begu and T. Desmettre, *Microvasc. Res.*, 1998, 55, 146-152.
26. L. B. Josefsen and R. W. Boyle, *Metal-Based Drugs*, 2008, 2008, 276109.
27. L. B. Josefsen and R. W. Boyle, *Theranostics*, 2012, 2, 916-966.
28. H. Ali and J. E. van Lier, *Chem. Rev.*, 1999, 99, 2379-2450.
29. C. K. Lim, J. Shin, Y. D. Lee, J. Kim, K. S. Oh, S. H. Yuk, S. Y. Jeong, I. C. Kwon and S. Kim, *Theranostics*, 2012, 2, 871-879.
30. S. Mathew, T. Murakami, H. Nakatsuji, H. Okamoto, N. Morone, J. E. Heuser, M. Hashida and H. Imahori, *ACS Nano*, 2013, 7, 8908-8916.
31. A. K. Singh, M. A. Hahn, L. G. Gutwein, M. C. Rule, J. A. Knapik, B. M. Moudgil, S. R. Grobmyer and S. C. Brown, *Int. J. Nanomed.*, 2012, 7, 2739-2750.
32. Y. H. Jin, F. M. Ye, M. Zeigler, C. F. Wu and D. T. Chiu, *ACS Nano*, 2011, 5, 1468-1475.
33. L. P. Song, H. Li, U. Sunar, J. Chen, I. Corbin, A. G. Yodh and G. Zheng, *Int. J. Nanomed.*, 2007, 2, 767-774.
34. N. M. Shao, Y. Z. Su, J. J. Hu, J. H. Zhang, H. F. Zhang and Y. Y. Cheng, *Int. J. Nanomed.*, 2011, 6, 3361-3372.
35. O. Taratula, C. Schumann, M. A. Naleway, A. J. Pang, K. J. Chon and O. Taratula, *Mol. Pharmaceut.*, 2013, 10, 3946-3958.
36. O. Taratula, O. B. Garbuzenko, P. Kirkpatrick, I. Pandya, R. Savla, V. P. Pozharov, H. X. He and T. Minko, *J. Control. Release*, 2009, 140, 284-293.
37. S. G. Kimani, T. A. Shmigol, S. Hammond, J. B. Phillips, J. I. Bruce, A. J. MacRobert, M. V. Malakhov and J. P. Golding, *Photochem. Photobiol.*, 2013, 89, 139-149.
38. Z. Wang, D. J. Coleman, G. Bajaj, X. Liang, G. Ganguli-Indra and A. K. Indra, *J. Investig. Dermatol.*, 2011, 131, 177-187.
39. S. Dayal, J. Li, Y. S. Li, H. Q. Wu, A. C. S. Samia, M. E. Kenney and C. Burda, *Photochem. Photobiol.*, 2008, 84, 243-249.
40. J. T. F. Lau, P. C. Lo, W. P. Fong and D. K. P. Ng, *Chem.-Eur. J.*, 2011, 17, 7569-7577.

41. N. Sekkat, H. van den Bergh, T. Nyokong and N. Lange, *Molecules*, 2012, 17, 98-144.
42. C. Kojima, Y. Toi, A. Harada and K. Kono, *Bioconjug. Chem.*, 2007, 18, 663-670.
43. D. Kannaiyan and T. Imae, *Langmuir*, 2009, 25, 5282-5285.
44. F. Wang, X. P. Cai, Y. Z. Su, J. J. Hu, Q. Wu, H. F. Zhang, J. R. Xiao and Y. Y. Cheng, *Acta Biomater.*, 2012, 8, 4304-4313.
45. G. M. Dykes, *J. Chem. Technol. Biot.*, 2001, 76, 903-918.
46. T. M. Allen and P. R. Cullis, *Science*, 2004, 303, 1818-1822.
47. J. A. Parrish, *J. Investig. Dermatol.*, 1981, 77, 45-50.
48. M. Katayose, S. Tai, K. Kamijima, H. Hagiwara and N. Hayashi, *J. Chem. Soc. Perk. T 2*, 1992, 403-409.
49. I. J. MacDonald and T. J. Dougherty, *J. Porphyr. Phthalocyan.*, 2001, 5, 105-129.
50. S. Tai and N. Hayashi, *J. Chem. Soc. Perk. T 2*, 1991, DOI: Doi 10.1039/P29910001637, 1275-1279.
51. S. Kim, M. Fujitsuka and T. Majima, *J. Phys. Chem. B*, 2013, 117, 13985-13992.
52. G. Hegyi, G. P. Szigeti and A. Szasz, *Evid.-Based Compl. Alt.*, 2013.
53. R. Tivony, L. Larush, O. Sela-Tavor and S. Magdassi, *J. Biomed. Nanotechnol.*, 2014, 10, 1041-1048.
54. X. H. Zheng, D. Xing, F. F. Zhou, B. Y. Wu and W. R. Chen, *Mol. Pharmaceut.*, 2011, 8, 447-456.
55. M. B. Zheng, C. X. Yue, Y. F. Ma, P. Gong, P. F. Zhao, C. F. Zheng, Z. H. Sheng, P. F. Zhang, Z. H. Wang and L. T. Cai, *Acs Nano*, 2013, 7, 2056-2067.
56. J. Yu, D. Javier, M. A. Yaseen, N. Nitin, R. Richards-Kortum, B. Anvari and M. S. Wong, *J. Am. Chem. Soc.*, 2010, 132, 1929-1938.
57. R. D. Almeida, B. J. Manadas, A. P. Carvalho and C. B. Duarte, *BBA-Rev. Cancer*, 2004, 1704, 59-86.
58. K. Low, T. Knobloch, S. Wagner, A. Wiehe, A. Engel, K. Langer and H. von Briesen, *Nanotechnology*, 2011, 22.
59. P. Agostinis, K. Berg, K. A. Cengel, T. H. Foster, A. W. Girotti, S. O. Gollnick, S. M. Hahn, M. R. Hamblin, A. Juzeniene, D. Kessel, M. Korbelik, J. Moan, P. Mroz, D. Nowis, J. Piette, B. C. Wilson and J. Golab, *CA-Cancer J. Clin.*, 2011, 61, 250-281.
60. S. L. Gibbs, *Quant. Imaging Med. Surg.*, 2012, 2, 177-187.
61. M. Krajewska, H. G. Wang, S. Krajewski, J. M. Zapata, A. Shabaik, R. Gascoyne and J. C. Reed, *Cancer Res.*, 1997, 57, 1605-1613.
62. M. Zhang, T. Murakami, K. Ajima, K. Tsuchida, A. S. D. Sandanayaka, O. Ito, S. Iijima and M. Yudasaka, *Proc. Natl. Acad. Sci. USA*, 2008, 105, 14773-14778.

## Figures Legends

**Figure 1.** (A) Chemical structures of parent silicon naphthalocyanine, silicon 2,3-naphthalocyanine dihydroxide (SiNcOH **1**) and substituted derivative, silicon 2,3-naphthalocyanine bis(trihexylsilyloxy) (SiNc **2**). (B) Schematic illustration of the fabrication of SiNc-loaded theranostic nanoplatform: 1) encapsulation of SiNc molecules within the hydrophobic interior of amine terminated generation 5 PPI dendrimers (PPIG5); 2) dendrimer surface modification with polyethylene glycol (PEG). The inset represents a photo of SiNc-NP solution in water.

**Figure 2.** (A) Normalized absorption spectra of SiNcOH-NP (red), and SiNc-NP (black) in 1X PBS buffer, and free SiNcOH **1** (green) and SiNc **2** (blue) in THF. (B) Fluorescence spectra of SiNcOH-NP (red), and SiNc-NP (black) in 1X PBS buffer,  $\lambda_{ex} = 770$  nm. The insets indicate fluorescence images of SiNcOH-NP and SiNc-NP in 1X PBS buffer recorded with Li-COR Pearl Animal Imaging System at 800 nm channel.

**Figure 3.** (A) Singlet oxygen generation by SiNcOH-NP (10  $\mu\text{g/mL}$ ) and SiNc-NP (10  $\mu\text{g/mL}$ ) before (dark) and after (light) NIR irradiation (785 nm laser diode, 0.3  $\text{W/cm}^2$ , 5 min). (B) Temperature change curves of water (black), SiNcOH-NP (red) in 1X PBS buffer, SiNc-NP (black) in 1X PBS buffer and free SiNc **2** (blue) in THF exposed to the 785 nm laser diode at a power density of 1.3  $\text{W/cm}^2$ . SiNc concentration in all the solutions was 100  $\mu\text{g/mL}$ . (C) Temperature change curves of SiNc-NP water solution (100  $\mu\text{g/mL}$ ) exposed to the 785 nm laser diode at the following power densities: 0.3 (red), 0.75 (black) and 1.3 (blue)  $\text{W/cm}^2$ .

**Figure 4.** Absorption spectra of aqueous solutions of SiNc-NP (**A**), and ICG (**B**) before and after irradiation with the 785 nm laser diode (785 nm, 1.3 W/cm<sup>2</sup>, 30 min, OD<sub>770</sub> = 1.2). The insets demonstrate light and fluorescence images of SiNc-NP and ICG water solutions before (left) and after (right) laser irradiation recorded with Li-COR Pearl Animal Imaging System at 800 nm channel. (**C**) Temperature change curves of optically matched (OD<sub>770</sub> = 0.5) aqueous solutions of SiNc-NP (blue), ICG (red) and water (black) exposed to the 785 nm laser diode at a power density of 1.3 W/cm<sup>2</sup>.

**Figure 5.** (**A**) Dark cytotoxicity and photodynamic (PDT) therapeutic effect of the prepared nanoplatfrom on A2780/AD ovarian cancer cells incubated with different concentrations of SiNc-NP and irradiated for 10 min using 785 nm laser diode (0.3 W/cm<sup>2</sup>). (**B**) Combinatorial (PDT+PTT) therapeutic effect of the prepared nanoplatfrom on A2780/AD ovarian cancer cell pellets incubated with SiNc-NP at a concentration of 25 µg/mL and irradiated for 10 min using 785 nm laser diode (1.3 W/cm<sup>2</sup>, yellow bar) compared to the next controls: (1) untreated cells (black bar) , (2) cells treated with SiNc-NP and SiNcOH-NP (25 µg/mL) under dark conditions (red and green bars), (3) untreated cells exposed to the laser diode (785 nm, 1.3 W/cm<sup>2</sup>, 10 min, blue bar), (4) photodynamic therapy only (SiNc-NP exposed to 0.3 W/cm<sup>2</sup> light, cyan bar), and (5) photothermal therapy only (SiNcOH-NP exposed to 1.3 W/cm<sup>2</sup> light, magenta bar). (**C**) Dynamic temperature profile of A2780/AD cells transfected with SiNc-NP (25 µg/mL) and exposed to the laser diode (785 nm, 1.3 W/cm<sup>2</sup>). Non-treated cells exposed to the laser diode were used as the control. The arrows indicate when the laser diode was turned on and off, respectively. (**D**) Relative intracellular ROS levels in A2780/AD cells incubated with SiNc-NP at a concentration of 25 µg/mL and irradiated for 10 min using the 785 nm laser diode (1.3 W/cm<sup>2</sup>).

Non-treated cells and cells treated with SiNc-NP under dark conditions were used as the controls.

**Figure 6.** In vivo imaging and combinatorial phototherapy studies of SiNc-NP. Representative light (A) and fluorescence (B) images of tumors-bearing mouse before injection with SiNc-NP (top images), after injection (middle) and 25 days after treatment (bottom) with the laser diode (785 nm, 1.3 W/cm<sup>2</sup>, 10 min). The left tumor was injected with SiNc-NP and exposed to the laser diode. The untreated right tumor was used as a control. (C) The fluorescence images of the cancer tumor acquired with the Li-COR Pearl Animal Imaging System before and after treatment with the laser diode (785 nm, 1.3 W/cm<sup>2</sup>, 10 min).

**Figure 7.** (A) Temperature changes inside the tumor treated with SiNc-NP and exposed to the 785 nm laser diode at a power density of 1.3 W/cm<sup>2</sup>. Untreated tumor exposed to the laser diode under the same experimental conditions was used as a control. The arrows indicate when the laser diode was turned on and off, respectively. (B) Tumor growth curves of different groups of mice after treatment. Error bars are based on standard deviations.

**Figure 8.** Tissue samples of control (untreated and NIR 1.3 W/cm<sup>2</sup> light only treated) tumor, tumor treated with SiNc-NP (SiNc-NP dark) and tumor treated simultaneously with SiNc-NP and NIR 1.3 W/cm<sup>2</sup> (SiNc-NP light) were stained with caspase-3, a marker of apoptosis, and DAPI (blue) staining showing total nuclei. Apoptotic cells appear in pink (indicated by arrow).

Figure 1

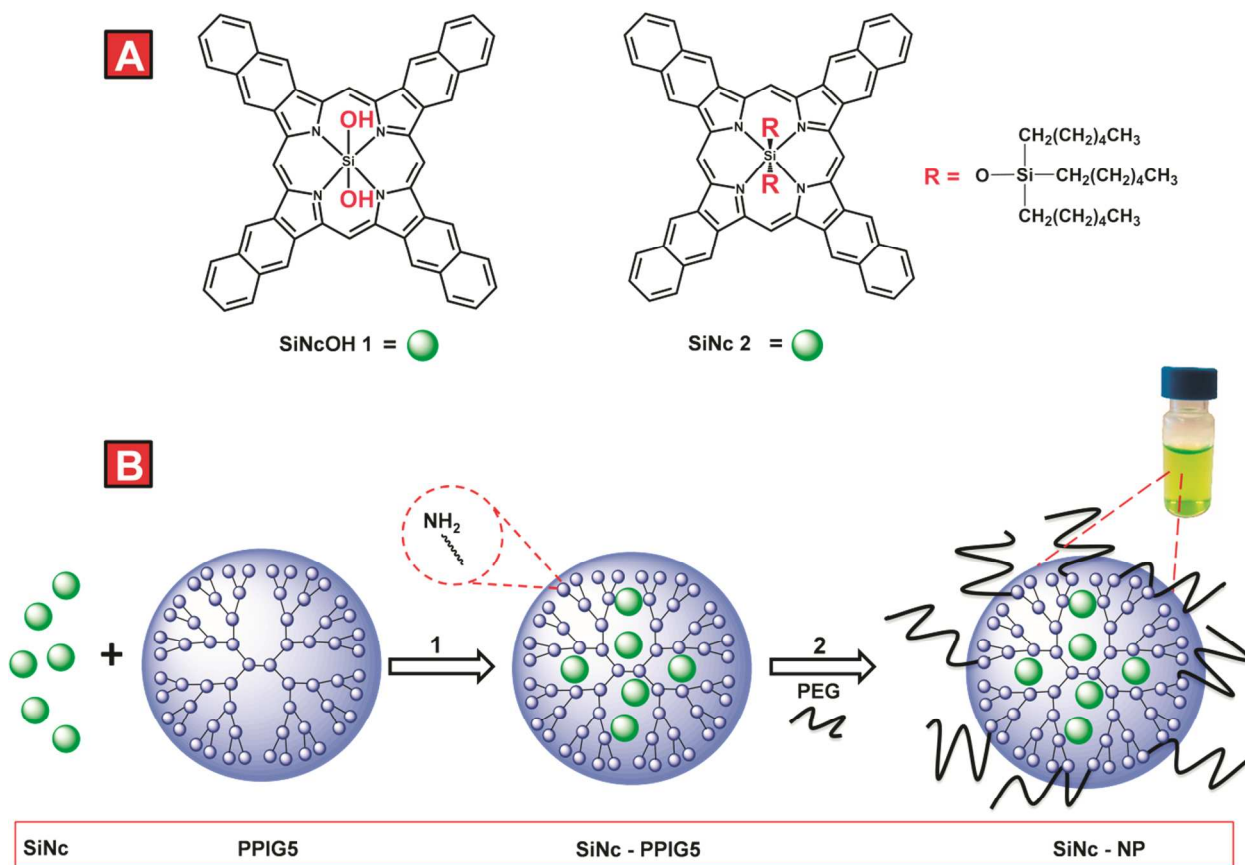


Figure 2

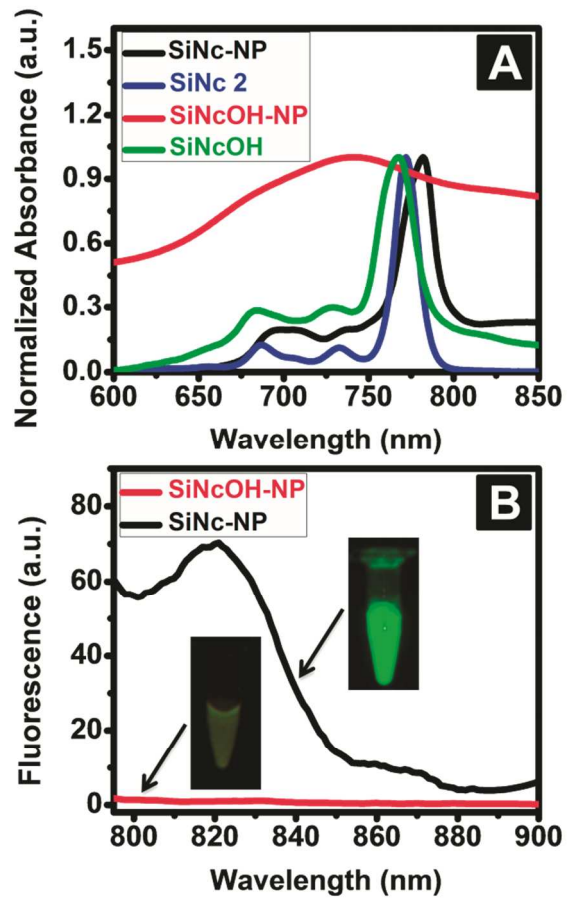


Figure 3

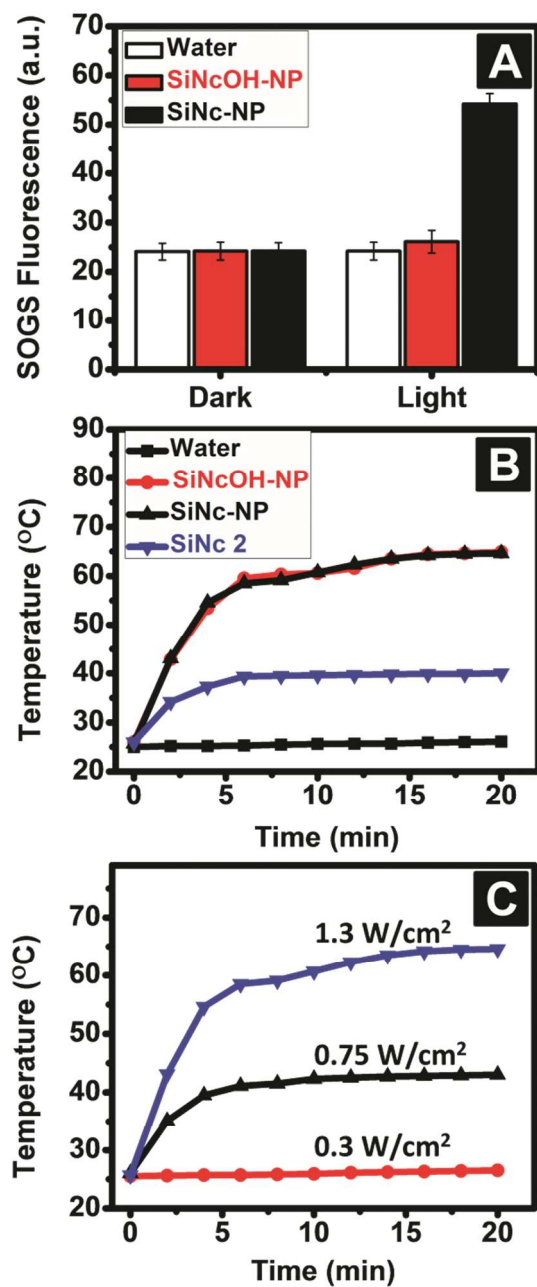


Figure 4

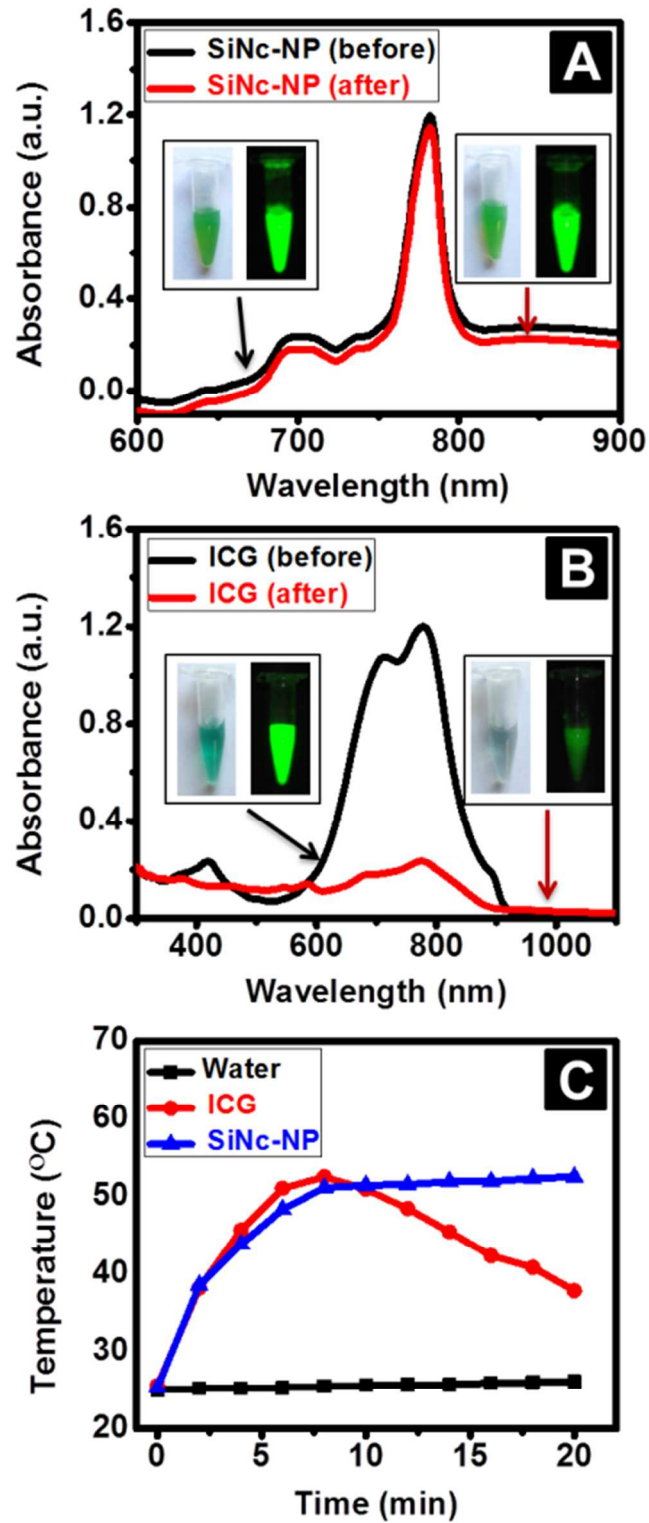


Figure 5

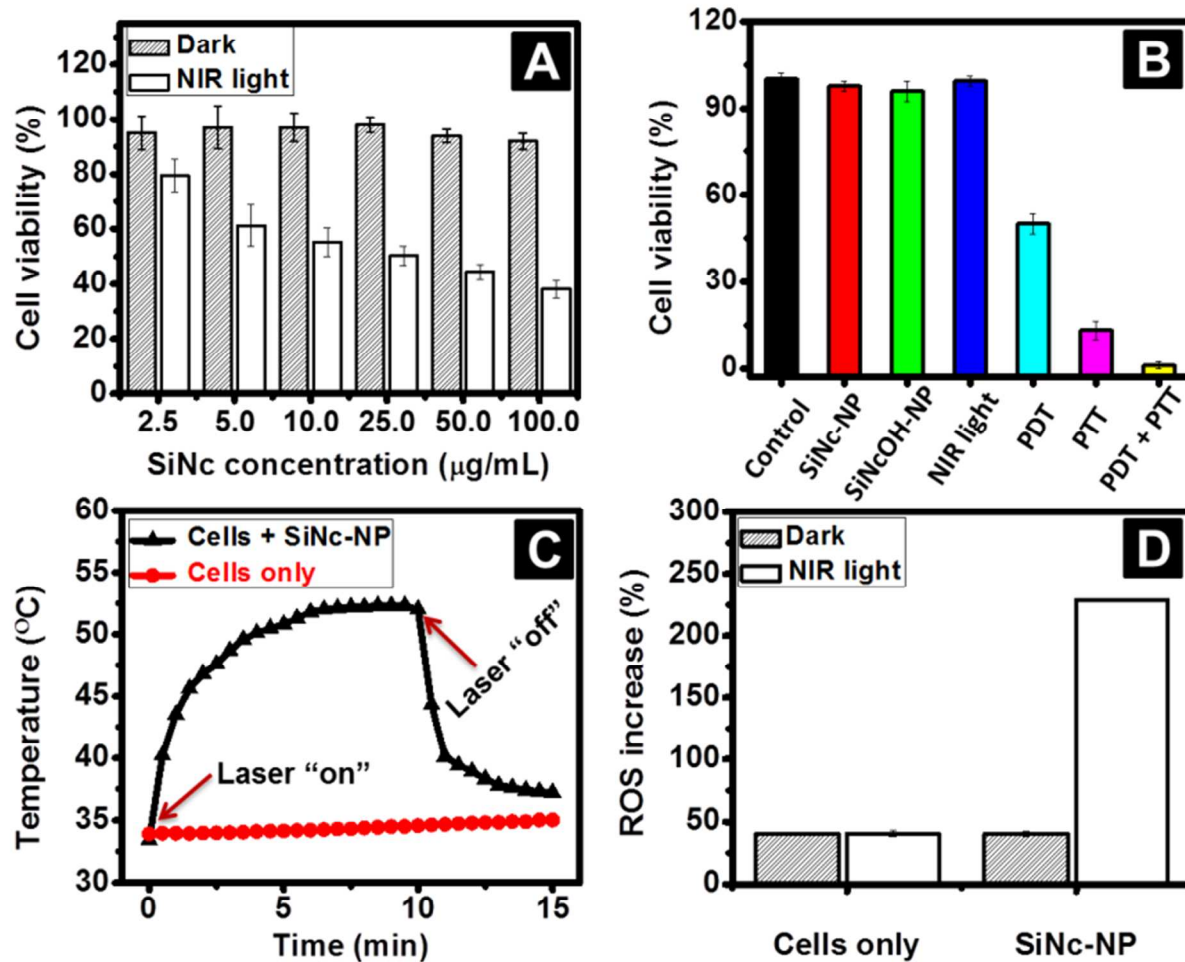


Figure 6

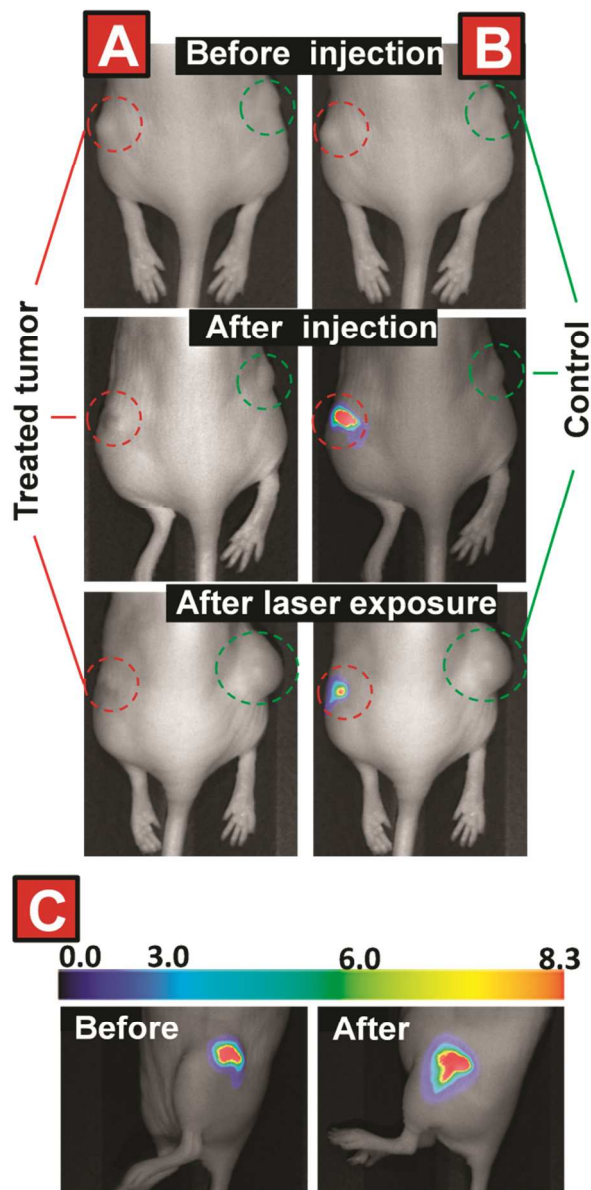


Figure 7

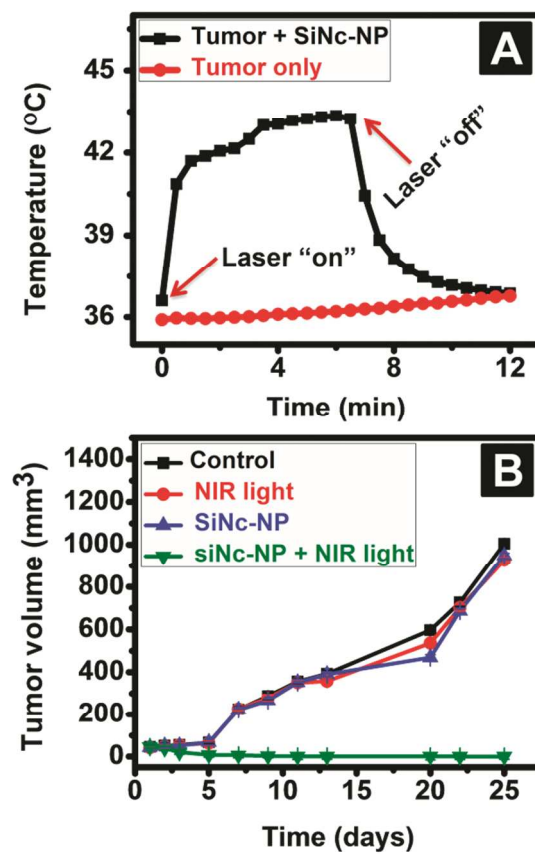


Figure 8

